Electrodeformation for single cell mechanical characterization

Electrodeformation for single cell mechanical characterization

Jian Chen[1], Mohamed Abdelgawad[2,5], Liming Yu[2], Nika Shakiba[1],
Wei-Yin Chien[1], Zhe Lu[2], William R Geddie[3], Michael A S Jewett[4]
and Yu Sun[1,2,6]

[1] Institute of Biomaterials and Biomedical Engineering, University of Toronto, Toronto, ON, M5S 3G8, Canada
[2] Department of Mechanical and Industrial Engineering, University of Toronto, Toronto, ON, M5S 3G8, Canada
[3] Department of Pathology, University of Toronto, Toronto, ON, M5G 2C4, Canada
[4] Department of Surgical Oncology, Princess Margaret Hospital, Toronto, ON, M5G 2M9, Canada

E-mail: sun@mie.utoronto.ca

Abstract

This paper presents the use of electrodeformation as a method for single cell mechanical characterization in which mechanical properties of SiHa and ME180 cells (two cervical cancer cell lines) were quantified. Cells were directly placed between two microelectrodes with a rectangular ac electric field applied, and cell deformation was recorded under certain experimental conditions. Numerical simulations were performed to model cell electrodeformation based on the Maxwell stress tensor formulation. In these simulations, effects of cell electrical property variations on their electrodeformed behavior were investigated. By comparing the measured morphological changes with those obtained from numerical simulations, we were able to quantify Young's modulus of SiHa cells (601 ± 183 Pa) and ME180 cells (1463 ± 649 Pa). These values were consistent with Young's modulus values (SiHa: 400 ± 290 Pa and ME180: 1070 ± 580 Pa) obtained from conventional micropipette aspiration.

S Online supplementary data available from stacks.iop.org/JMM/21/054012/mmedia

(Some figures in this article are in colour only in the electronic version)

1. Introduction

The mechanical behavior of biological cells is largely determined by their cytoskeleton [1, 2]. Abnormal cellular functions can change cytoskeletons and lead to mechanical property variations [3, 4]. Differences in mechanical properties of cells have been shown to correlate with pathophysiological states in many diseases such as arthritis [5], asthma [6], malaria [7, 8], sickle cell anemia [9, 10] and cancer [11–13].

Particularly in the specific topic of human cancer, numerous studies have shown that the stiffness of metastatic cancer cells are significantly lower than that of benign cells [11–13] due to their altered cytoskeletal organization. Cross *et al* have pointed out that even though cancer is tremendously biochemically diverse, a common range of Young's modulus for each cell type is exhibited even for different tumor types and patient effusions [11]. This evidence suggests that differences in mechanical properties at the cellular level can potentially be used as a cue in cancer detection.

Several well-known characterization tools have been used to measure mechanical properties of single cells such as atomic force microscopy (AFM), micropipette aspiration, optical tweezers and magnetic bead microrheometry [14, 15]. In AFM, a sharp tip at the free end of a flexible cantilever generates a local deformation on the cell surface. The resulting deflection of the cantilever reflects the cell's mechanical

1

properties. In micropipette aspiration, a cell is deformed by applying suction through a micropipette placed on the surface of the cell. By recording geometrical changes of the cell, the elastic response of the cell is inferred. In optical tweezers, dielectric beads are attached to the opposite ends of a cell to allow for cell elongation triggered by optical forces, followed by measurement of the mechanical properties. In magnetic bead microrheometry, functionalized beads are attached to a cell and a magnetic field imposes a twisting moment on the beads, thereby deforming a portion of the cell. In all these techniques, forces are applied over small areas of the cell which result in local characterization of cell properties.

Compared to other techniques, electrodeformation [16–19] is more amenable for lab-on-a-chip implementation. On-chip electrodeformation does not require dedicated infrastructure while other techniques such as AFM, micropipette aspiration, and laser tweezers require more sophisticated setups. Additionally, it is possible to realize mechanical testing of cells in parallel using this lab-chip technique.

Electrodeformation was first demonstrated in 1984 when Engelhardt *et al* [16] reported the relationship between applied voltages and corresponding deformation ratios of erythrocytes. Later, they used the same setup to calculate the Young's modulus of erythrocyte plasma membranes by treating cells as conductive spheres (they neglected membrane polarization) [17]. Zimmermann *et al* [19] reported the relationship between applied voltages and corresponding electrodeformation ratios of cells via microfabricated electrodes, however, without interpreting raw data (voltage deformation) into cells' Young's modulus. In a recent study, MacQueen *et al* [18] calculated the elastic properties of cells using the Clausius–Mossotti factor with the effective dipole moment assumption, which is only valid when the scale of the electric field non-uniformity is large compared to cell dimensions. In such case, the cell in the electric field is treated as an infinitesimal charged particle whose presence has no disturbance on the electric field between two microelectrodes. In the case of electrodeformation with a cell settled down on one electrode tip (equilibrium location), it is under highly non-uniform electric field and the effective dipole moment approximation can lead to significant errors [20].

Although electrodeformation was demonstrated more than two decades ago, the technique was only used in a limited number of studies because several critical questions remain unanswered. For example, the effect of cells' electrical property variations on the electrical forces experienced by the cells is still not well understood. Furthermore, due to the complexity of the physical phenomena involved, there is no direct closed-form mathematical expression that relates the applied electric field to the cellular mechanical stiffness. In this study, we developed a microdevice for mechanical characterization of SiHa and ME180 cells using electrodeformation. Single cells were deformed under an applied ac electric field and corresponding deformations were measured under certain experimental conditions. Numerical simulations were used to evaluate the applied electrodynamic forces based on the Maxwell stress tensor formulation [21],

which is suitable to treat a wide range of applied electric fields. In these simulations, the relationship between applied voltages and deformation ratios of cells with different Young's moduli was investigated. By comparing experimentally measured deformations with those obtained from numerical simulations, we were able to quantify the Young's modulus of SiHa and ME180 cells.

2. Materials and methods

2.1. Materials

Unless otherwise indicated, all chemicals were obtained from Sigma-Aldrich (Oakville, ON, Canada) and cell-culture reagents were from American Type Culture Collection (ATCC, Manassas, VA, USA). Materials required for device fabrication included indium-tin oxide (ITO)-coated glass substrates (Delta Technologies Ltd, Stillwater, MN, USA), Shipley S1818 photoresist and MF321 developer (Rohm and Haas, Marlborough, MA, USA). Bovine serum albumin (BSA) (Invitrogen Canada, Burlington, ON, Canada) was used in the electrodeformation experiment.

2.2. Experimental procedures

2.2.1. Device fabrication. ITO was chosen as the electrode material because it is transparent and facilitates inverted microscopy imaging. Microelectrodes were fabricated in the clean room facility of the Emerging Communications Technology Institute at the University of Toronto. Glass slides coated with 200 nm ITO were cleaned in acetone, methanol and DI water, and dried on a hotplate (30 min at 150 °C). A 200 nm thick layer of silicon dioxide was deposited on ITO glass slides (5 min at 400 °C, deposition rate: 40 nm min^{-1}) using a plasma enhanced chemical vapor deposition (PECVD) system (Oxford Instruments, UK) (see figure 1(*a*)).

Shipley S1818 photoresist was spun on the slide (4000 rpm for 45 s), soft baked (1 min at 115 °C), and exposed to UV light (10 s, 16 mW cm^{-2}, 365 nm) through a chrome-on-glass mask (University of Alberta Nanofabrication facility, Alberta, Canada) using a Karl Suss MA6 mask aligner (Garching, Germany). Slides were then developed in MF321 developer for 60 s, and finally hard baked (1 h at 120 °C).

Silicon dioxide without protection from the patterend photoresist was etched away using an inductive coupled plasma/reactive ion etching system (Trion Technology, FL, USA) with CHF$_3$ as the etchant gas (2 min, etch rate: 100 nm min^{-1}). The exposed ITO was then etched away in a solution (HCl:HNO$_3$:H$_2$O 55:7.5:32.5 mL) to pattern the microelectrodes (2 min at 50 °C). The residual photoresist was removed in acetone and the residual silicon dioxide was removed by using CHF$_3$ again as mentioned before.

2.2.2. Preparation of cell suspension. SiHa and ME180 cells were purchased from American Type Culture Collection (Manassas, VA, USA) and cultured in Eagle's Minimum Essential Medium supplemented with 10% fetal bovine serum and McCoy's 5a Medium Modified supplemented with 10%
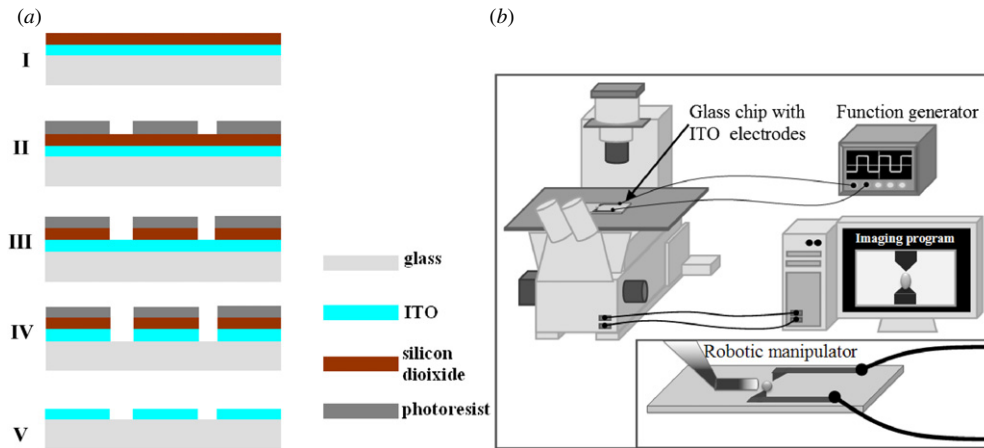
Figure 1. (*a*) Fabrication steps for ITO based microelectrodes. (*b*) The experimental setup for cell electrodeformation testing. A cell is directly placed on top of the electrodes. Rectangular ac signals are applied, and cell deformation images are captured and processed.

fetal bovine serum, respectively. Cells were cultured on tissue culture-treated polystyrene flasks and immediately prior to an experiment, cells were trypsinized, centrifuged and resuspended in isotonic sucrose solutions of 10.2% (weight to volume) plus 0.01% BSA. Sucrose, extensively used in experimental setups requiring positive dielectrophoresis (pDEP), was used as the cell suspension medium for its low conductivity [22, 23]. 0.01% BSA was added to decrease the adhesion between cells and the substrate in the experiment [24].

2.2.3. Device operation. A droplet of the suspending solution was pipetted onto the electrode of the microdevice and single SiHa or ME180 cells were placed on the tip of one of the electrodes, using a home developed automatic robotic manipulation platform [25]. Robotic placement of sinlge cells on the electrode eliminated the need for single cell trapping techniques. Rectangular ac signals were generated from a function generator (Model# 4040A B&K Precision Corp., CA, USA) for electrodeformation experiments (figure 1(*b*)). A minimal ac signal (3 V for the functional generator we used) was applied to attract single cells to the tip of one electrode (equilibrium location). If no cell lysis was noticed, the applied voltage was increased 2 V per step and kept steady for 30 s, with deformation pictures of cells taken. Then the voltage was increased again in the same manner until cell lysis was noticed. Three different frequencies of 500 kHz, 1 MHz, and 5 MHz were used in this experiment.

In order to quantify the geometric differences in electrodeformed cells, a sub-pixel ellipse extraction algorithm was developed to process the captured images. The procedure consists of a sequence of standard image processing steps adapted to the context of cell electrodeformation (such as smoothing, thresholding, edge detection, followed by a Hough transform) [26]. The direction and the lengths of deformation along the semimajor and semiminor axes were obtained from the algorithm that calculates the deformation ratio.

2.2.4. Conventional micropipette aspiration for cell mechanical characterization. To verify our electrodeformation technique, conventional micropipette aspiration experiments were conducted on SiHa and ME180 cells. In the setup, a borosilicate glass micropipette tip (5 μm diameter) was held by a micromanipulator (Sutter Instrument Company, CA, USA) mounted on an inverted phase-contrast microscope. Attached to the pipette glass tube was an in-house voltage-controlled vacuum source generator (a minimum pressure resolution of 8 Pa).

The experiment started with the submersion of the micropipette tip inside the cell-containing medium and the positioning of the tip close to the surface of a target cell. Then, a small negative pressure (usually 20–50 Pa) was applied in order to immobilize the cell and to form a complete seal. From this reference state, subsequent larger suction pressures were then applied and images of the aspirated cell were captured. The Young's modulus of the aspirated cell was estimated from a common biomechanics model that approximates a cell as an elastic half-space solid (linear, homogeneous and incompressible) [27, 28] using the following equation [14]:

$$E = \frac{3}{2\pi} \frac{\Delta P}{\phi} \frac{R_p}{L} \qquad (1)$$

where E is the Young's modulus for the cell, ΔP is the applied sucking pressure, L is the aspiration length, R_p is the radius of pipette, and ϕ is a constant with a typical value of 2.1.

2.3. Numerical analysis

Extensive simulations were conducted using the finite element analysis package COMSOL 3.4 (Burlington, MA, USA) to quantify the Young's modulus from experimental data (voltage deformation). First, the electric field was calculated in the cell vicinity, and electrodynamic forces exerted on the cell were computed by integrating the Maxwell stress tensor over the cell surface. Second, a value of Young's modulus of the cell was assumed, and the calculated electrodynamic forces were used as a load to calculate cell deformation. Finally, the calculated deformations at different values of Young's modulus were
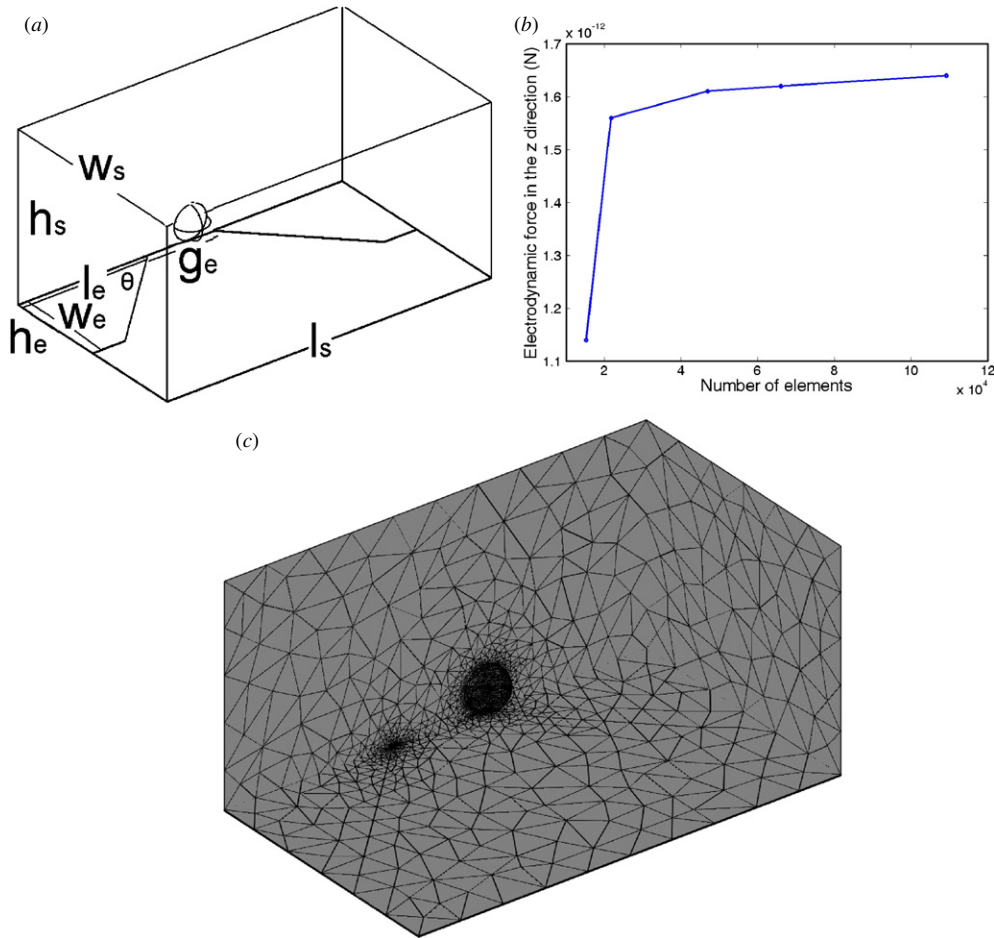
Figure 2. (*a*) Schematic of the numerical model used in the simulations. Half geometry was simulated to reduce mesh size. All variables are defined with specific values listed in table 1. (*b*) Electrodynamic forces (integration of the Maxwell stress tensor around cell membrane in the *z*-direction) as a function of the number of elements. A mesh independent solution was achieved at ∼40 000 elements. The simulation conditions are as follows: 1 V$_{p-p}$, surrounding medium conductivity of 10^{-3} S m^{-1}, cell membrane relative permittivity of 20, cytoplasm conductivity of 0.4 S m^{-1} and cytoplasm relative permittivity of 80. (*c*) A picture of meshing with 40 000 elements.

compared with experimental results under the same conditions and an approximate value of the Young's modulus of the cell was extracted.

2.3.1. Geometrical parameters and physical properties. Figure 2(*a*) and table 1 show the electrode and cell dimensions used in this study. The optimum overall dimensions of the surrounding medium were determined by evaluating a series of cases with different lengths, widths and heights. We started with a large model and then reduced the model size gradually until a size was reached, which was large enough to simulate infinite space with reasonable accuracy without unnecessary waste of computational time. The optimum size had the following dimensions: length 100 μm, width 60 μm and height 50 μm (see supplementary figure S1 available at stacks.iop.org/JMM/21/054012/mmedia). Since the model is symmetric, half the geometry was simulated to minimize the number of elements.

Since exact electrical properties of SiHa and ME180 cells are not known, we simulated a range of electrical properties of cells reported previously in the literature, table 2 [29–36], to determine their effects on generated electrodynamic

Table 1. Electrode dimensions and relevant parameters used in numerical simulation.

Parameter	Value
Electrode length (l_e)	40 μm
Electrode width (w_e)	30 μm
Electrode tip angle (θ)	45°
Electrode tip gap (g_e)	20 μm
Electrode height (h_e)	0.2 μm
Cell diameter (d_c)	10 μm
Cell membrane thickness (t_c)	10 nm
Cell center height (h_c)	5.3 μm
Simulation model length (l_s)	100 μm
Simulation model height (h_s)	50 μm
Simulation model width (w_s)	60 μm

forces. Ranges of cell electrical properties tested were as follows: membrane relative permittivity $\varepsilon_{membrane}$ of 10, 20 and 30, cytoplasm relative permittivity $\varepsilon_{cytoplasm}$ of 40, 80 and 120, and cytoplasm conductivity $\sigma_{cytoplasm}$ of 0.1, 0.4 and 0.7 S m^{-1}. In the electric field simulation, a quasi-static electric model (ac/dc module) was used, with the governing equations and boundary conditions shown as follows.

Table 2. Electrical properties of cells from previous publications. The ranges of cell electrical properties used in this simulation are as follows: membrane relative permittivity of 10–30, cytoplasm conductivity of 0.1–0.7 S m^{-1} and cytoplasm relative permittivity of 40–150.

Cell type	Cell properties		
	$\sigma_{\text{cytoplasm}}$ (S m^{-1})	$\varepsilon_{\text{cytoplasm}}$	C_{membrane} (mF m^{-2})
Red blood cell [29]	0.52 ± 0.051	57 ± 5.4	9 ± 0.8
T-lymphocyte [29]	0.76 ± 0.058	64 ± 5.9	11 ± 1.1
T-lymphocyte [30]	0.65 ± 0.15	103.9 ± 24.5	10.5 ± 3.1
B-lymphocyte [30]	0.73 ± 0.18	154.4 ± 39.9	12.6 ± 3.5
Monocyte [30]	0.56 ± 0.10	126.8 ± 35.2	15.3 ± 4.3
Granulocyte [30]	0.60 ± 0.13	150.9 ± 39.3	11.0 ± 3.2
Fiend murine erythroleukemia DS19 [29]			14.7 ± 2.0
Human promyelocytic leukemia cell HL-60 [30]			15 ± 1.9
Human promyelocytic leukemia cell HL-60 [35]			15.6 ± 0.9
Human chronic myelogeneous leukemia K562 [32]	0.30 ± 0.02		9.7 ± 0.9
Human chronic myelogeneous leukemia K562 [36]	0.28		
Human chronic myelogeneous leukemia K562 [31]	0.23 ± 0.01		9.8 ± 0.8
Human breast cancer MDA-231 [29]	0.62 ± 0.073	52 ± 7.3	25.9 ± 3.7
Human breast cancer MDA-435 [29]			13.5 ± 1.9
Human breast cancer MDA-468 [29]			27.5 ± 4.2
Human breast cancer MCF-7 [34]	0.23 ± 0.01		12.4 ± 1.8
Human breast cancer MCF-7TaxR [34]	0.14 ± 0.01		20.6 ± 1.1
Human breast cancer MCF-7DoxR [34]	0.40 ± 0.02		12.4 ± 0.9
Human breast cancer MCF-7MDR1 [34]	0.27 ± 0.02		12.6 ± 0.7
Human oral squamous cell carcinoma H357 [33]	0.31 ± 0.02		18.9 ± 2.5
Human HPV-16 transformed keratinocyte UP [33]	0.45 ± 0.05		11.4 ± 0.6

2.3.2. Governing equations. In the case of a cell exposed to a non-uniform electric field, the electromechanics of the cell is modeled as an electrodynamic force exerted upon a lossy dielectric spherical shell containing a linear and isotropic conductive sphere, which is submersed in a lossy dielectric medium.

The electrostatic characteristics were obtained by solving the equation of continuity for the conduction and displacement currents by explicitly showing its frequency dependence

$$-\nabla \cdot ((\sigma + j\omega\varepsilon_r\varepsilon_0)\nabla\phi) = 0, \tag{2}$$

where σ denotes the electrical conductivity of the cell, ω is the angular frequency of the driving field, $\varepsilon = \varepsilon_r\varepsilon_0$ is the permittivity (ε_r is the relative permittivity of the medium and ε_0 is that of vacuum) and ϕ is the electric potential. The electric field $\mathbf{E}$ and the displacement $\mathbf{D}$ can be obtained from the gradient of the potential ϕ:

$$\mathbf{E} = -\nabla\phi \tag{3}$$

$$\mathbf{D} = \varepsilon_r\varepsilon_0\mathbf{E}. \tag{4}$$

The electrodynamic force $\mathbf{F}$ assuming negligible magnetic contributions [37], upon the cell volume V, enclosed by a closed surface S, due to the applied external electric field $\mathbf{E}$, at each point on S, is given by

$$\mathbf{F} = \int_V \left[\varepsilon\,(\nabla \cdot \mathbf{E})\,\mathbf{E} + \varepsilon(\mathbf{E} \cdot \nabla)\mathbf{E} - \frac{1}{2}\nabla(\varepsilon\mathbf{E} \cdot \mathbf{E}) \right] dV. \tag{5}$$

This equation can be further simplified by using a tensor notation and transforming the volume integral to a surface integral via the Gauss theorem. The resulting equation for the force per unit area exerted on the surface of the cell becomes

$$\mathbf{F} = \oint_S \mathbf{T} \cdot \mathbf{n}\,dS \tag{6}$$

$$T_{ij} = \varepsilon\left(E_i E_j - \frac{1}{2}\delta_{ij}E^2 \right) \tag{7}$$

with T_{ij} as the nine components of the Maxwell stress tensor (the indices i and j refer to pairs of x-, y- and z-axes and δ_{ij} is the Kronecker delta). The three diagonal elements of T_{ij} are known to represent pressures while the off-diagonal elements represent shears [21]. The unit vector $\mathbf{n}$ is normal to the surface.

It is important to note that by employing the Maxwell stress tensor, there is no underlying assumptions on the non-uniformity of the electric field as is needed for the effective dipole moment method frequently used in dielectrophoretic force calculation [20]. As a result, our approach is more general and can more accurately predict electrodynamic forces on the cell in regions of high field non-uniformity as is the case when the cell is at the tip of one of the electrodes [20].

2.3.3. Boundary conditions. The driving potential was applied to the left electrode while ground potential was applied to the right one. The other external boundaries were electrically insulated ($\mathbf{n} \cdot \mathbf{J} = 0$) to meet the requirement of charge conservation, equation (2), where $\mathbf{J}$ is the current density. Boundary conditions on the plane of symmetry were set to satisfy equation (2). At interfaces between the cell surface and the internal/external medium, continuity of the electric field $\mathbf{E}$, electric displacement $\mathbf{D}$ and current density $\mathbf{J}$ were applied according to

$$\mathbf{n} \cdot (\mathbf{D}_1 - \mathbf{D}_2) = \rho_s, \qquad \mathbf{n} \times (\mathbf{E}_1 - \mathbf{E}_2) = 0 \qquad \text{and}$$
$$\mathbf{n} \cdot (\mathbf{J}_1 - \mathbf{J}_2) = 0, \tag{8}$$

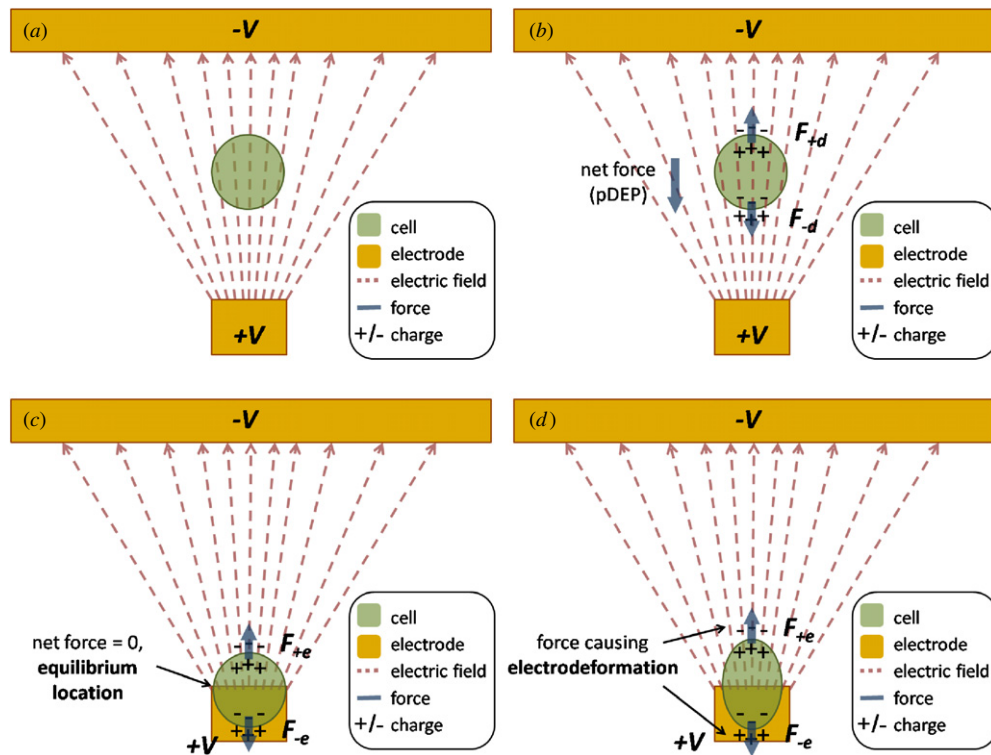where ρ_s is the surface charge density.

Figure 3. Schematic of positive dielectrophoresis (pDEP) and electrodeformation. (*a*) Cell is placed in a non-uniform electric field. (*b*) Cell is more polarizable than the surrounding medium in the case of pDEP with imbalanced DEP forces (F_{+d} and F_{-d}) on two hemi-ellipsoids. In such a case, cell is pushed to move toward higher electric field density. (*c*) Cell settles down at equilibrium location (the highest electric field region) with balanced DEP forces (F_{+e} and F_{-e}) on two hemi-ellipsoids with zero net force. (*d*) These same distributed forces on cell halves lead to elongation of the cell at equilibrium location.

2.3.4. Numerical methods. We used a Lagrange-quadratic element type and the PARDISO direct solver [38] for electric simulations and the GMRES iterative stationary solver [39] with geometric multigrid preconditioner for mechanical simulations. The relative tolerance used as a convergence criterion was

$$\rho |M^{-1}(b - Ax)| < \text{tol.} |M^{-1}b|, \qquad (9)$$

where ρ is the factor in error estimation ($\rho = 400$ in this study), M is the preconditioner matrix, $Ax = b$ is the system of equations to be solved, and tol. $= 10^{-6}$ is the relative tolerance.

2.3.5. Mesh independence. In initial tests, different meshes were employed to optimize the mesh size that yields a solution independent of discretization. Figure 2(*b*) shows the effect of number of elements on the electrodynamic forces acting in the *z*-direction, as an integration of the Maxwell stress tensor along the cell surface. As shown, convergence was reached at about 40 000 elements (figure 2(*c*)).

3. Results and discussion

When a cell suspended in a conductive medium is subjected to an electric field (figure 3), charges are trapped on cell surface and therefore an electrodynamic force distribution is applied on the cell. If the electric field is non-uniform and the relative polarizability of the cell is higher than that of the medium, this force distribution has a net resultant leading to cell translation toward areas of higher electric fields (i.e. pDEP). In such a

case, the cell moves and settles down on one electrode tip (i.e. the highest electric field region) where the electrodynamic force on the cell is balanced out. Although the resultant force distribution in the plane of motion is zero at this location, the distributed forces on the two cell halves lead to elongation of the cell in a phenomenon called electrodeformation. The amount of cell deformation induced depends on the magnitude of the electrodynamic forces generated (which in turn depends on the applied electric field and the cell-medium electrical properties) and on the cell stiffness.

Electrodeformation can only be observed under pDEP, where the cells anchor on one of the electrodes under the electrodynamic forces in the negative *z*-direction (i.e. downward forces). To achieve pDEP with the highest electrodynamic force possible, proper choice of medium properties and applied frequency is crucial. A low medium conductivity is required to make the cell more polarizable [20] to induce pDEP. The lower the medium conductivity relative to that of the cell cytoplasm, the higher the electrodynamic force, which is due to the larger difference in the electric field inside and outside the cell. The low medium conductivity also results in a larger voltage drop across the medium rather than across the cell membrane, which decreases the possibility of electrolysis.

Choice of the frequency of the applied electric field is of utmost importance. In dc or low frequency fields, the dielectric cell membrane acts like an insulator and bears the most of the voltage drop resulting in cell lysis at low applied
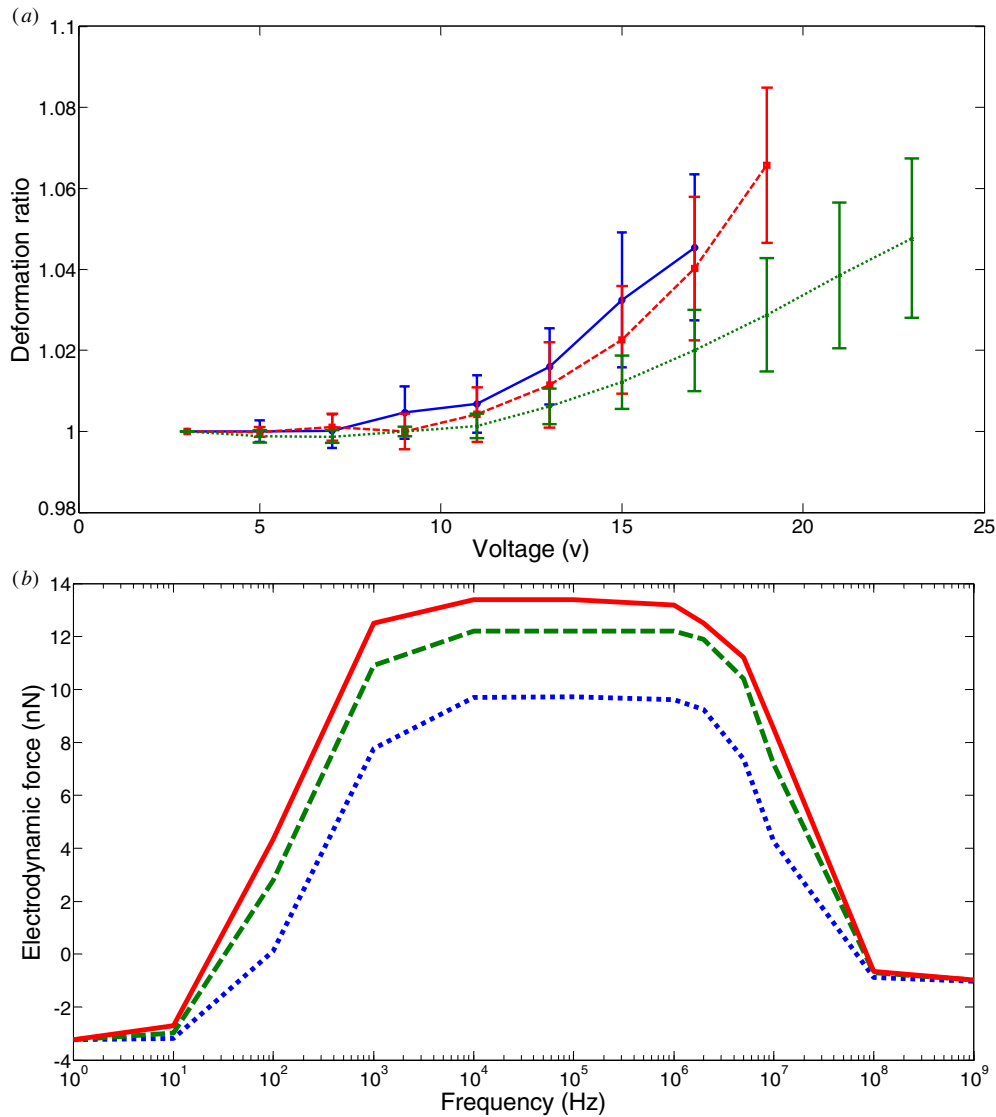
Figure 4. (a) Experimental electrodeformation of SiHa cells as a function of electric field strength with an applied electric field of frequency 500 kHz, 1 MHz and 5 MHz. Sample size is five cells at 500 kHz (blue), seven cells at 1 MHz (red) and five cells at 5 MHz (green). The deformation ratio is defined as the ratio between the elongation of the cell parallel to the applied electric field direction and the original diameter of the cell before electrodeformation. (b) Electrodynamic forces as a function of frequency at 19 V_{p-p} under surrounding medium conductivity of 10^{-3} S m^{-1} with the following electrical properties: $\varepsilon_{membrane} = 10$, $\sigma_{cytoplasm} = 0.1$ S m^{-1}, $\varepsilon_{cytoplasm} = 40$ (red); $\varepsilon_{membrane} = 20$, $\sigma_{cytoplasm} = 0.4$ S m^{-1}, $\varepsilon_{cytoplasm} = 80$ (green) and $\varepsilon_{membrane} = 30$, $\sigma_{cytoplasm} = 0.7$ S m^{-1}, $\varepsilon_{cytoplasm} = 120$ (blue).

potentials. Whereas at very high frequencies when the effect of permittivity dominates over that of conductivity, the cell membrane becomes electrically transparent, making the cell behave more like a homogeneous cytoplasm, with the same permittivity as the surrounding medium resulting in smaller electrodynamic forces. Thus we used a frequency range of 100 kHz to 10 MHz which generates high electrodynamic forces and results in a shorter time duration per cycle for charge build-up on the cell surface, and thus reduces the electrolysis effect [19, 40].

3.1. Cell elongation

Three frequencies: 500 kHz, 1 MHz and 5 MHz were chosen to deform cells electrically with the surrounding medium conductivity of 10^{-3} S m^{-1} (see figure 4(a)). The deformation

ratio is defined as the ratio between the elongation of the cell parallel to the applied electric field direction and the original diameter of the cell before electrodeformation. In the experiment, the applied voltage was increased in steps of 2 V and kept steady for 30 s per step, with cell deformation pictures recorded until electrolysis occurred.

As shown in figure 4(a), the cell lysis voltage increased from 19 to 25 V as the applied frequency was increased from 500 kHz to 5 MHz, which agreed well with the theoretical analysis on cell electrolysis discussed previously. Under the same voltage, the deformation ratios of cells at 500 kHz and 1 MHz were comparable while the deformation ratios of cells at 5 MHz were significantly lower, suggesting that 5 MHz is beyond the upper frequency limit to generate highest electrodynamic forces possible. This was confirmed by simulation results which show a decline in the electrodynamic
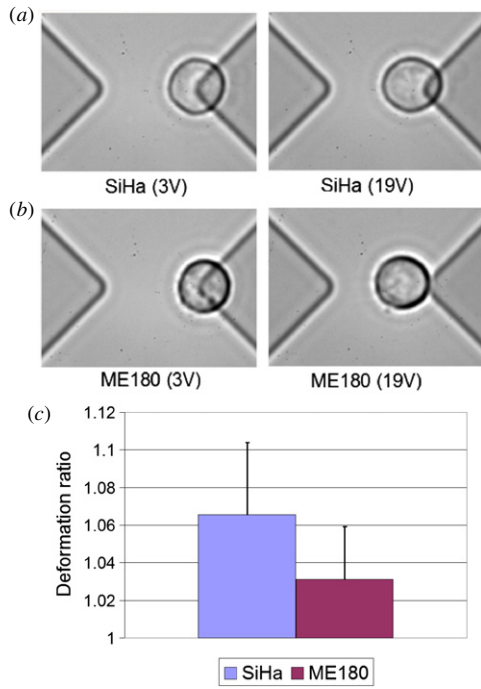
(*a*)

SiHa (3V)   SiHa (19V)

(*b*)

ME180 (3V)   ME180 (19V)

(*c*)

Figure 5. Top: images of electrodeformation of SiHa (*a*) and
ME180 (*b*) cells as a function of electric field strength using a cell
suspension of sucrose with 0.01% BSA, electric field frequency of
1 MHz, and electrode gap of 20 μm. Applied electric field strength
is indicated in brackets. (*c*) Electrodeformation ratio of SiHa and
ME180 cells at 19 V_{p-p} at 1 MHz with electrode gap of 20 μm.
Sample size is seven cells per cell line.

force value at frequencies higher than 1 MHz regardless of cell
electrical properties (see figure 4(*b*)).

When subjected to electric fields, both SiHa and ME180
cells showed elongation parallel to the applied electric field
lines. The deformation ratio of SiHa and ME180 cells was
respectively 1.066 ± 0.0254 and 1.031 ± 0.0257 at 19 V_{p-p}
indicating a lower stiffness for SiHa cells (see figure 5).

3.2. Effect of cells' electrical properties

The value of the electrodynamic forces generated on cells
cannot be exactly predicted unless the electrical properties
of the cell (i.e. cytoplasm permittivity and conductivity and
membrane permittivity) are known. Since electrical properties
of SiHa and ME180 cells are not known, the electrodynamic
forces were calculated at a range of cell electrical properties of
21 different types of cells (table 2). Twenty-seven independent
simulations were performed to include all permutations of the
electrical parameters $\varepsilon_{\text{membrane}} = \{10, 20, 30\}$, $\varepsilon_{\text{cytoplasm}} = \{40,
80, 120\}$ and $\sigma_{\text{cytoplasm}} = \{0.1, 0.4, 0.7\}$ S m^{-1}.

As shown in table 3, for a cell with unknown electrical
properties, the simulated electrodynamic force fell into the
range of 11.54 nN $\pm$ 1.55 nN, by calculating the average
and the standard deviation of the electrical simulation results
of 27 cases mentioned above. The simulated maximum
electrodynamic force was 13.45 nN (16.5% higher than the
average value) and the minimal electrodynamic force was
9.17 nN (20.5% lower than the average value).

Table 3. Simulation results of the effect of different cell electrical
properties on electrodynamic forces for cell deformation by
integrating the Maxwell stress tensor along the cell membrane in the
equilibrium location. Simulations were conducted with the electric
field of 1 MHz, 19 V_{p-p} and the surrounding medium conductivity
of 10^{-3} S m^{-1}. Cell electrical property variations are as follows:
$\varepsilon_{\text{membrane}} = 10$–$30$, $\sigma_{\text{cytoplasm}} = 0.1$–$0.7$ S m^{-1}, $\varepsilon_{\text{cytoplasm}} = 40$–$120$.

Cell electrical property			
$\varepsilon_{\text{membrane}}$	$\varepsilon_{\text{cytoplasm}}$	$\sigma_{\text{cytoplasm}}$ (S m^{-1})	Electrodynamic force (nN)
10	40	0.1	9.32
10	40	0.4	9.70
10	40	0.7	9.72
10	80	0.1	9.24
10	80	0.4	9.69
10	80	0.7	9.72
10	120	0.1	9.17
10	120	0.4	9.69
10	120	0.7	9.71
20	40	0.1	11.61
20	40	0.4	12.23
20	40	0.7	12.22
20	80	0.1	11.50
20	80	0.4	12.21
20	80	0.7	12.28
20	120	0.1	11.14
20	120	0.4	12.22
20	120	0.7	12.22
30	40	0.1	12.26
30	40	0.4	13.45
30	40	0.7	13.44
30	80	0.1	12.51
30	80	0.4	13.42
30	80	0.7	13.41
30	120	0.1	12.24
30	120	0.4	13.34
30	120	0.7	13.34
		Average	11.54
		Standard deviation	1.55

Among these three studied parameters, membrane
permittivity had the largest effect on the generated
electrodynamic force with an increase of 31% when
membrane relative permittivity increased from 10 to 30, (see
figure 6(*a*)). Cytoplasm conductivity had a moderate effect
on generated forces which increased by 9% when cytoplasm
conductivity increased from 0.1 to 0.7 S m^{-1}, whereas
cytoplasm permittivity had negligible effect on electrodynamic
forces. The electrodynamic force in this context is the
integration of the Maxwell stress tensor over one-half of the
cell in the *x*-direction (i.e. cell elongation direction) at
the equilibrium location. A cell's equilibrium location was
defined as the location on top of the electrode where the net
x-forces vanish. Since the equilibrium location changed with
different electrical properties tested, new equilibrium points
had to be found for each new set of parameters.

3.3. Calculation of Young's modulus

By comparing the calculated deformations at different values
of Young's modulus with experimental results, the Young's
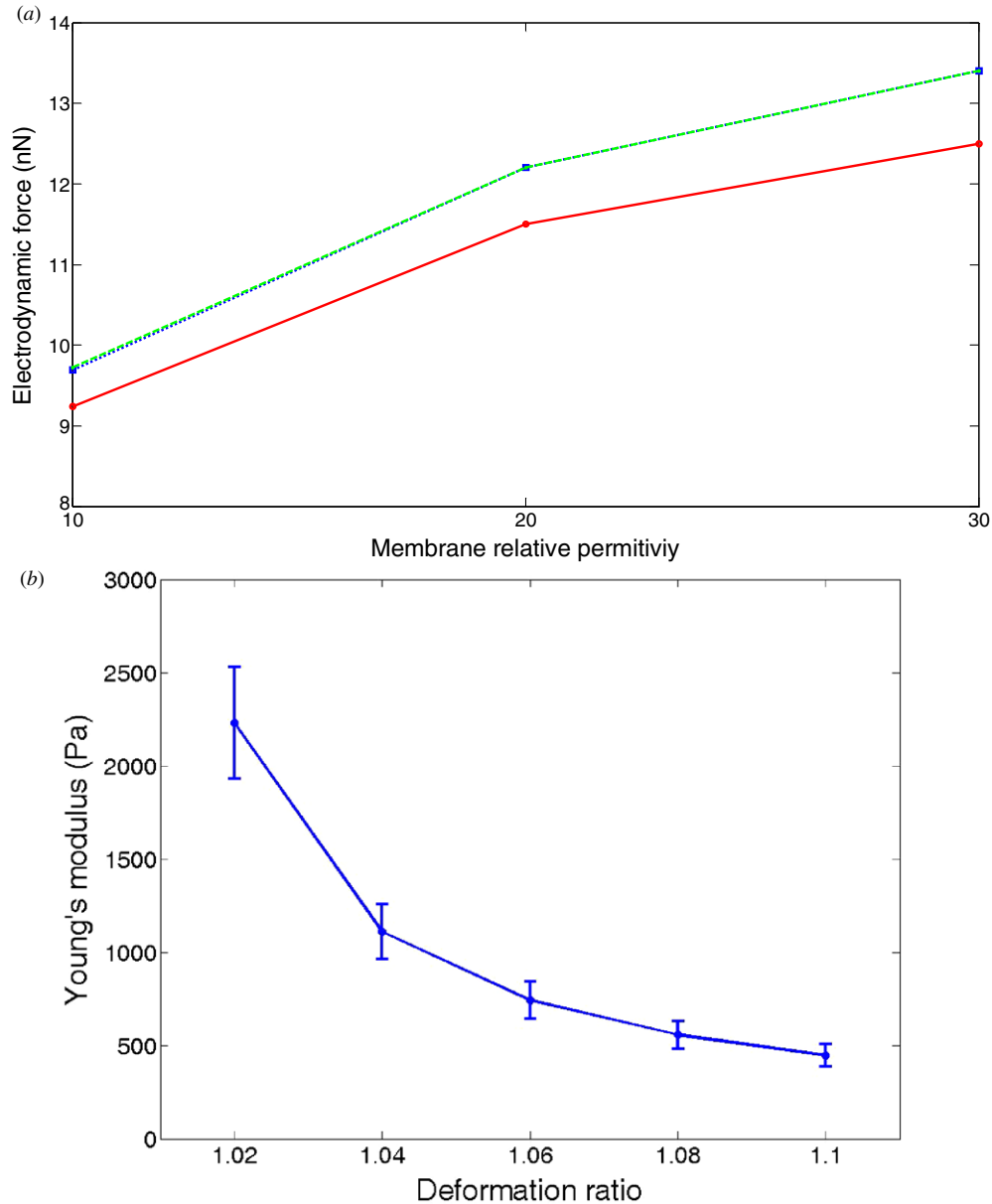modulus of the cell was determined. Since a range of

Figure 6. (*a*) Simulation results of electrodynamic forces as a function of membrane relative permittivity $\varepsilon_{\text{membrane}}$ ($\sigma_{\text{cytoplasm}} = 0.1$ (red), 0.4 (blue) and 0.7 S m^{-1} (green), $\varepsilon_{\text{cytoplasm}} = 80$). (*b*) Young's modulus calculation as a function of the deformation ratio from numerical simulations. For a given deformation ratio, 27 Young's modulus values were obtained based on simulation results, which reflected 27 cases of electrical property variations shown in table 3. The standard deviations (within 15% of the average value) represented the range of Young's modulus values due to cell electrical property variations. Simulations were conducted with the electric field of 1 MHz and the surrounding medium conductivity of 10^{-3} S m^{-1}.

electrodynamic forces was calculated for each case due to the uncertainty in cell electrical properties, Young's modulus was calculated as lying between a minimum and maximum value for each deformation ratio measured.

As shown in figure 6(*b*), for a deformed cell with electrical properties unknown, Young's modulus from simulations fell into the following ranges: 2289 ± 299 Pa (deformation ratio: 1.02), 1115 ± 149 Pa (deformation ratio: 1.04), 743 ± 99 Pa (deformation ratio: 1.06), 557 ± 75 Pa (deformation ratio: 1.08) and 446 ± 60 Pa (deformation ratio: 1.10) respectively, by calculating 27 values of Young's modulus (corresponding to 27 cases of different electrical properties) for a given

deformation ratio. Overall, the standard deviations were within 15% of the averages.

The deformation ratios of individual SiHa and ME180 cells collected from experiments were used to fit the simulation results as mentioned above for Young's modulus calculation (see supplementary figure S2 available at stacks.iop.org/JMM/21/054012/mmedia). For each cell with a measured deformation ratio, 27 values of Young's modulus were calculated and represented by the average and the standard deviation. As shown in figure 7, individual SiHa and ME180 cells showed different Young's modulus values, which were due to cell heterogeneity.
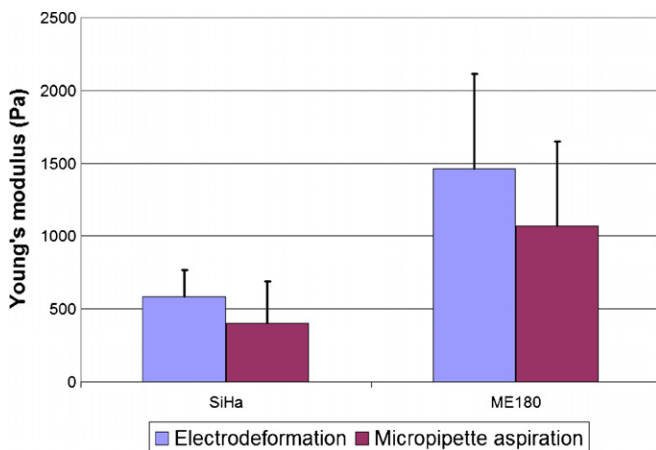
Figure 7. Comparison between the Young's modulus values of SiHa and ME180 cells determined from electrodeformation and micropipette aspiration. Sample size is seven cells per cell line. Electrodeformation was conducted at 19 V_{p-p} and 1 MHz. Standard deviation bars of electrodeformation are mainly due to the effect of cell electrical property variations from numerical simulations and cell stiffness variations among individual cells from experiments.

Young's modulus was quantified from electrodeformation to be 601 ± 183 Pa for SiHa cells, and 1463 ± 649 Pa for ME180 cells (see figure 7). The average and the standard deviation of Young's modulus were calculated from 189 values per cell line corresponding to seven experimentally deformed cells in which for each deformed cell, there were 27 Young's modulus values due to different electrical properties. Conventional micropipette aspiration was used to verify Young's modulus values calculated using electrodeformation. Values of Young's modulus found were 400 ± 290 Pa for SiHa cells and 1070 ± 580 Pa for ME180 cells (see supplementary figure S3 available at stacks.iop.org/JMM/21/054012/mmedia).

4. Conclusion

This paper demonstrated the use of electrodeformation of biological cells as a method to quantify mechanical properties. Electrodeformation experiments were conducted to deform SiHa and ME180 cells under applied electric fields, in which they were distinguished based on different deformation ratios. Simulation results demonstrated the effect of cell electrical property variations on the relationship between applied voltages and deformations of cells with different Young's modulus. By comparing the experimentally measured deformations with those obtained from numerical simulations, we were able to quantify Young's modulus of SiHa (601 ± 183 Pa) and ME180 cells (1463 ± 649 Pa), which were consistent with Young's modulus values (SiHa: 400 ± 290 Pa and ME180: 1070 ± 580 Pa) obtained from conventional micropipette aspiration. Further work will focus on the characterization of single cells' electrical and mechanical properties simultaneously by integrating electrodeformation with impedance measurements to further decouple the combined effect of cells' electrical and mechanical properties on their electrodeformed behavior.

References

[1] Boal D H 2002 *Mechanics of the Cell* (Cambridge: Cambridge University Press)
[2] Ethier C R and Simmons C A 2007 *Introductory Biomechanics: From Cells to Organisms* (Cambridge: Cambridge University Press)
[3] Lee G Y and Lim C T 2007 Biomechanics approaches to studying human diseases *Trends Biotechnol.* **25** 111–8
[4] Suresh S 2007 Biomechanics and biophysics of cancer cells *Acta Biomater.* **3** 413–38
[5] Trickey W R, Lee G M and Guilak F 2000 Viscoelastic properties of chondrocytes from normal and osteoarthritic human cartilage *J. Orthop. Res.* **18** 891–8
[6] An S S, Fabry B, Trepat X, Wang N and Fredberg J J 2006 Do biophysical properties of the airway smooth muscle in culture predict airway hyperresponsiveness? *Am. J. Respir. Cell Mol. Biol.* **35** 55–64
[7] Nash G B, O'Brien E, Gordon-Smith E C and Dormandy J A 1989 Abnormalities in the mechanical properties of red blood cells caused by Plasmodium falciparum *Blood* **74** 855–61
[8] Suresh S, Spatz J, Mills J P, Micoulet A, Dao M, Lim C T, Beil M and Seufferlein T 2005 Connections between single-cell biomechanics and human disease states: gastrointestinal cancer and malaria *Acta Biomaterialia* **1** 15–30
[9] Brandao M M, Fontes A, Barjas-Castro M L, Barbosa L C, Costa F F, Cesar C L and Saad S T 2003 Optical tweezers for measuring red blood cell elasticity: application to the study of drug response in sickle cell disease *Eur. J. Haematol.* **70** 207–11
[10] Nash G B, Johnson C S and Meiselman H J 1984 Mechanical properties of oxygenated red blood cells in sickle cell (HbSS) disease *Blood* **63** 73–82
[11] Cross S E, Jin Y S, Rao J and Gimzewski J K 2007 Nanomechanical analysis of cells from cancer patients *Nat. Nanotechnol.* **2** 780–3
[12] Guck J *et al* 2005 Optical deformability as an inherent cell marker for testing malignant transformation and metastatic competence *Biophys. J.* **88** 3689–98
[13] Lekka M, Laidler P, Gil D, Lekki J, Stachura Z and Hrynkiewicz A Z 1999 Elasticity of normal and cancerous human bladder cells studied by scanning force microscopy *Eur. Biophys. J.* **28** 312–6
[14] Kim D H, Wong P K, Park J, Levchenko A and Sun Y 2009 Microengineered platforms for cell mechanobiology *Annu. Rev. Biomed. Eng.* **11** 203–33
[15] Lim C T, Zhou E H, Li A, Vedula S R K and Fu H X 2006 Experimental techniques for single cell and single molecule biomechanics *Mater. Sci. Eng.* C **26** 1278–88
[16] Engelhardt H, Gaub H and Sackmann E 1984 Viscoelastic properties of erythrocyte membranes in high-frequency electric fields *Nature* **307** 378–80
[17] Engelhardt H and Sackmann E 1988 On the measurement of shear elastic moduli and viscosities of erythrocyte plasma

10

membranes by transient deformation in high frequency electric fields *Biophys. J.* **54** 495–508

[18] MacQueen L A, Buschmann M D and Wertheimer M R 2010 Mechanical properties of mammalian cells in suspension measured by electro-deformation *J. Micromech. Microeng.* **20** 065007 1–11

[19] Zimmermann U, Friedrich U, Mussauer H, Gessner P, Hamel K and Sukhoruhov V 2000 Electromanipulation of mammalian cells: fundamentals and application *IEEE Trans. Plasma Sci.* **28** 72–82

[20] Jones T B 1995 *Electromechanics of Particles* (Cambridge: Cambridge University Press)

[21] Griffiths D J 1999 *Introduction to Electrodynamics* 3rd edn (Upper Saddle River, NJ: Prentice Hall)

[22] Gray D S, Tan J L, Voldman J and Chen C S 2004 Dielectrophoretic registration of living cells to a microelectrode array *Biosens. Bioelectron.* **19** 1765–74

[23] Taff B M and Voldman J 2005 A scalable addressable positive-dielectrophoretic cell-sorting array *Anal. Chem.* **77** 7976–83

[24] Wheeler A R, Throndset W R, Whelan R J, Leach A M, Zare R N, Liao Y H, Farrell K, Manger I D and Daridon A 2003 Microfluidic device for single-cell analysis *Anal. Chem.* **75** 3581–6

[25] Lu Z, Moraes C, Ye G, Simmons C A and Sun Y 2010 Single cell deposition and patterning with a robotic system *PLoS One* **5** e13542 1–9

[26] Forsyth D and Ponce J 2003 *Computer Vision: A Modern Approach* (Upper Saddle River, NJ: Prentice Hall)

[27] Evans E A and La Celle P L 1975 Intrinsic material properties of the erythrocyte membrane indicated by mechanical analysis of deformation *Blood* **45** 29–43

[28] Hochmuth R M 2000 Micropipette aspiration of living cells *J. Biomech.* **33** 15–22

[29] Gascoyne P R C, Wang X B, Huang Y and Becker R F 1997 Dielectrophoretic separation of cancer cells from blood *IEEE Trans. Ind. Appl.* **33** 670–8

[30] Yang J, Huang Y, Wang X, Wang X B, Becker F F and Gascoyne P R 1999 Dielectric properties of human leukocyte subpopulations determined by electrorotation as a cell separation criterion *Biophys. J.* **76** 3307–14

[31] Chin S, Hughes M P, Coley H M and Labeed F H 2006 Rapid assessment of early biophysical changes in K562 cells during apoptosis determined using dielectrophoresis *Int. J. Nanomedicine* **1** 333–7

[32] Labeed F H, Coley H M and Hughes M P 2006 Differences in the biophysical properties of membrane and cytoplasm of apoptotic cells revealed using dielectrophoresis *Biochim. Biophys. Acta* **1760** 922–9

[33] Broche L M, Bhadal N, Lewis M P, Porter S, Hughes M P and Labeed F H 2007 Early detection of oral cancer—Is dielectrophoresis the answer? *Oral Oncol.* **43** 199–203

[34] Coley H M, Labeed F H, Thomas H and Hughes M P 2007 Biophysical characterization of MDR breast cancer cell lines reveals the cytoplasm is critical in determining drug sensitivity *Biochim. Biophys. Acta* **1770** 601–8

[35] Huang C, Chen A, Wang L, Guo M and Yu J 2007 Electrokinetic measurements of dielectric properties of membrane for apoptotic HL-60 cells on chip-based device *Biomed. Microdevices* **9** 335–43

[36] Duncan L, Shelmerdine H, Hughes M P, Coley H M, Hubner Y and Labeed F H 2008 Dielectrophoretic analysis of changes in cytoplasmic ion levels due to ion channel blocker action reveals underlying differences between drug-sensitive and multidrug-resistant leukaemic cells *Phys. Med. Biol.* **53** N1–7

[37] Mognaschi E R and Savini A 1983 The action of a non-uniform electric field upon lossy dielectric systems—ponderomotive force on a dielectric sphere in the field of a point charge *J. Phys. D: Appl. Phys.* **16** 1533–41

[38] Schenk O, Gärtner K, Fichtner W and Stricker A 2001 PARDISO: a high-performance serial and parallel sparse linear solver in semiconductor device simulation *Future Gener. Comput. Syst.* **18** 69–78

[39] Saad Y and Schultz M H 1986 Gmres—a generalized minimal residual algorithm for solving nonsymmetric linear-systems *SIAM J. Sci. Stat. Comput.* **7** 856–69

[40] Sukhorukov V L, Mussauer H and Zimmermann U 1998 The effect of electrical deformation forces on the electropermeabilization of erythrocyte membranes in low- and high-conductivity media *J. Membr. Biol.* **163** 235–45